 doi:10.20944/preprints201612.0133.v1

Article

MoS_2 Nanosheets Encapsulated in Carbon Nanofibers as Binder-free Anode for Superior Lithium Storage

Yakai Deng [1], Liang Zhan [1,*], Yanli Wang [1] and Shubin Yang [2,*]

[1] State Key Laboratory of Chemical Engineering, East China University of Science and Technology, Shanghai 200237, China; dengyakai126@163.com (Y.D.); ylwang@ecust.edu.cn (S.Y.)

[2] Key Laboratory of Aerospace Advanced Materials and Performance of Ministry of Education, School of Materials Science and Engineering, Beihang University, Beijing 100191, China

[*] Correspondence: zhanliang@ecust.edu.cn (L.Z.); yangshubin@buaa.edu.cn (S.Y.)

Abstract: The one-dimensional MoS_2/carbon nanofibers (1D MoS_2/CNFs) are synthesized by electrospinning using exfoliated MoS_2 nanosheets and polyacrylonitrile as raw materials. The exfoliated MoS_2 nanosheets with size of about 150 nm are encapsulated in carbon nanofibers, and the free-standing MoS_2/CNFs can be easily cut into flexible tablet and directly used as binder-free anode for lithium storage. The resultant 1D MoS_2/CNFs exhibit a very high reversible capacity of 700 mAh g^{-1} at 100 mA g^{-1} after 50 cycles, high rate capacity (450 mAh g^{-1} at 1000 mA g^{-1} after 200 cycles) and good cycle stability.

Keywords: MoS_2; carbon nanofibers; electrospinning; anode material

 doi:10.20944/preprints201612.0133.v1

1. Introduction

Lithium ion batteries (LIBs) have been regarded as one of the most important rechargeable energy storage devices with broad applications in hybrid and electric vehicles owing to their high potentials and environmental friendliness[1-3]. Owing to the low theoretical capacity of graphite (372 mAh g-1)[4], the reversible capacities of commercial graphite based anode materials cannot satisfy the increasing requirements for high-performance LIBs. Therefore, many endeavours have been concentrated on exploring novel anode materials, such as transition metal oxides[5], molybdenum disulfide (MoS_2)[6], stannum (Sn)[7], and silicon (Si)[8]. Among the novel anode candidates, MoS_2 has been recognized as one of the most promising and attractive one for LIBs, owing to its high theoretical capacity (670 mAh g-1), relatively low discharge potential, low-cost, safety and environment-friendly[9-11]. However, bulk MoS_2 suffers from a low electrical conductivity and volume expansion during cycle process, leading to poor electrochemical performance[10]. To overcome these shortcomings, researchers focus on fabricating single-layer or few layered MoS_2 by chemical vapor deposition[11,12], chemical exfoliation[13] and mechanical exfoliation [14,15]. Unconsideration the extremely low yield, the single-layer MoS_2 or MoS_2 nanosheets are easy to restack, leading to the structural instability during cycling, as a result, obvious volume expansion will occur and bring up rapid capacity fading[16]. Thus researcher further focus their attentions on

 doi:10.20944/preprints201612.0133.v1

combining MoS_2 nanostructures with carbonaceous materials (such as carbon nanotubes[17], grapheme[18,19], and conductive polymers[20]) to resolve the low electrical conductivity, volume change and restacking. However, how to develop a simple and efficient approach to fabricate MoS_2/carbon nanostructures is still a big challenge.

Herein, we develop an efficient approach to fabricate one-dimensional MoS_2/carbon nanofibers (denoted as 1D MoS_2/CNFs) by electrospinning. Exfoliated MoS_2 nanosheets with small lateral size were encapsulated in carbon nanofibers. The distinctive structure of 1D MoS_2/CNFs can improve the electrical conductivity of pure MoS_2 nanosheets, but also can prevent the restacking of nanosheets. Importantly, the free-standing MoS_2/CNFs can be easily cut into flexible film and directly used as binder-free anode for lithium storage. The unique structures offer the resultant 1D MoS_2/CNFs exhibit excellent electrochemical performance. For instance, the resultant 1D MoS_2/CNFs has a high volumetric capacity of 700 mAh g^{-1} at 100 mA g^{-1} after 50 cycles and good high-rate performance (450 mAh g^{-1} at 1000 mA g^{-1} after 200 cycles). We believe that this efficient method can be further extended to fabricate other active nanomaterials encapsulated in carbon nanofiber or carbon nanotube for broad applications in batteries, supercapacitors and catalysts.

2. Results and discussion

Figure 1 illustrates schematically the synthetic procedure of MoS_2/CNFs. Bulk MoS_2 were added to the deionized water and IPA solvent with a volume ratio of 1:1,

Preprints (www.preprints.org) | NOT PEER-REVIEWED | Posted: 28 December 2016 doi:10.20944/preprints201612.0133.v1

and exfoliated by emulsification machine at 10000 rpm. Subsequently, the exfoliated MoS_2 nanosheets were treated through freeze-drying, and then dispersed in the PAN/DMF solution. After the free-standing 1 D MoS_2/PAN based nanofibers were achieved by electrospinning, they were oxidized at 280 °C for 2 h and then carbonized at 850 °C for 3 h under Ar atmosphere, resulting in the 1D MoS_2/CNFs.

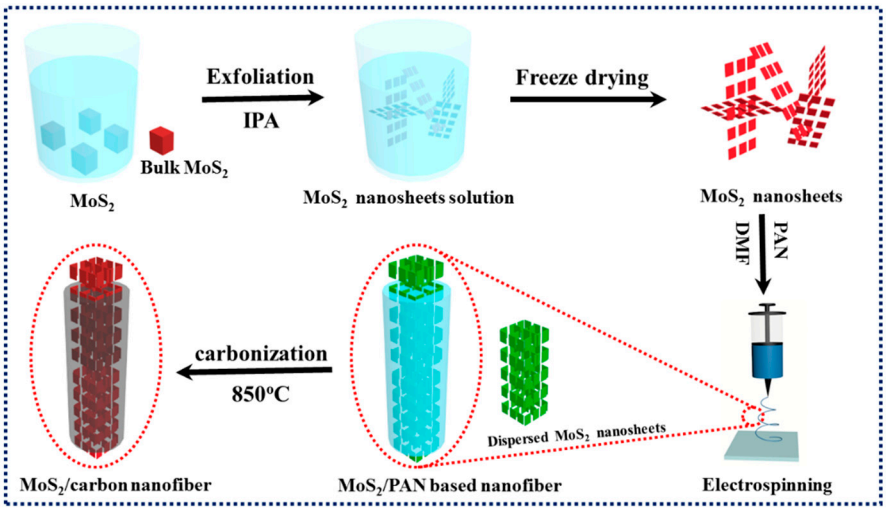

Figure 1. Schematic illustration of the fabrication of 1D MoS_2/CNFs

The MoS_2 nanosheets were achieved by solvent exfoliation with the lateral size of about 150 nm (Figure S1), and the exfoliated MoS_2 nanosheets can disperse well in the DMF solvent even after ten days (Figure S2). Subsequently, 1D MoS_2/CNFs were also successfully fabricated by electrospinning. As shown in Figure 2a, a large amount of interlaced one-dimensional MoS_2/CNFs are observed, and the nanofibers are uniform dispersed and have a diameter of about 180 nm. The surface of resultant MoS_2/CNFs is quite smooth, and no bulk MoS_2 or restacked MoS_2 nanosheets are detected among the nanofibers (Figure 2b), illustrating all the exfoliated MoS_2 nanosheets are encapsulated in the matrix of CNFs due to their small sizes and good affinity with PAN molecule. The TEM image in Figure 2c also shows that the nanofibers have uniform diameter

 doi:10.20944/preprints201612.0133.v1

with the size of about 180 nm,

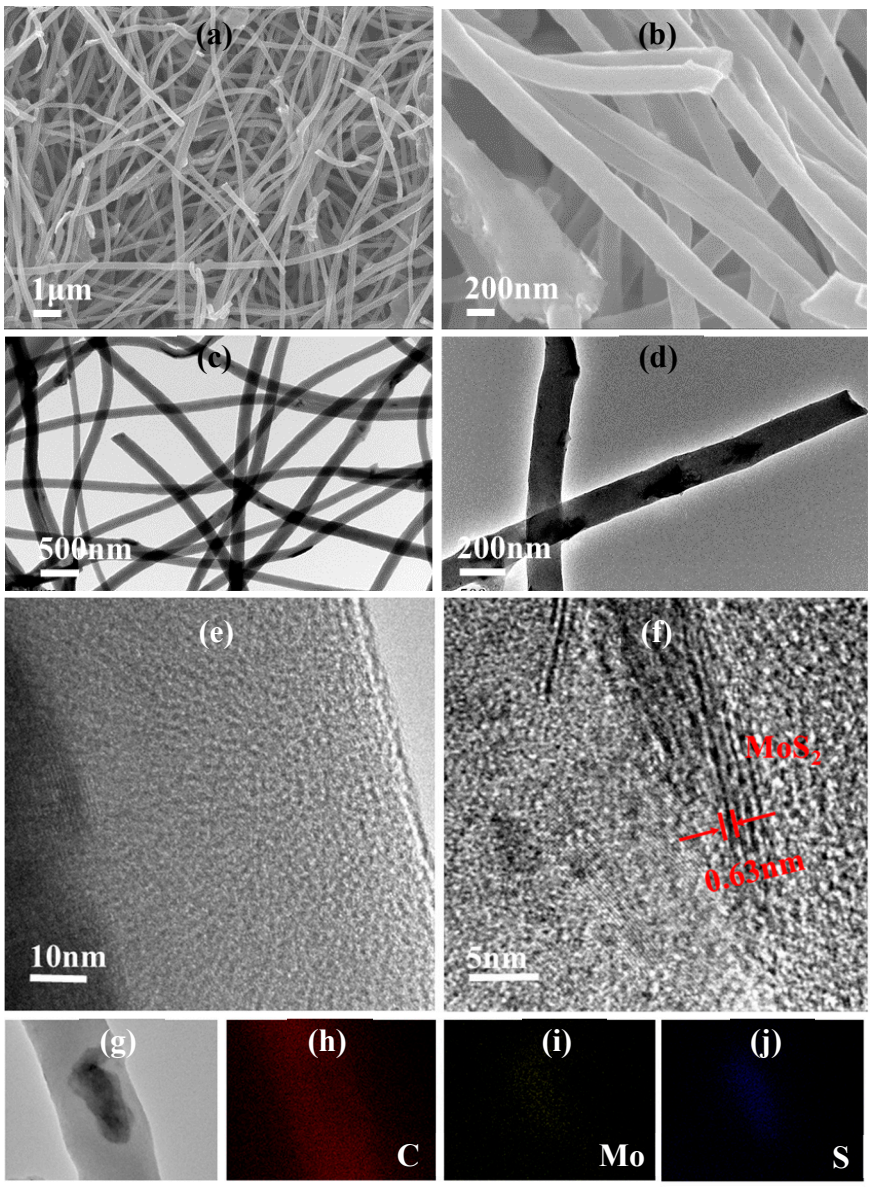

agreeing well with the results observed in the SEM image

 doi:10.20944/preprints201612.0133.v1

Figure 2. SEM **(**a, b), TEM (c, d) and HRTEM (e, f) images of synthesized 1D MoS_2/CNFs. (g) STEM image of 1D MoS_2/CNFs and its corresponding C (h), Mo (i) and S (j) elemental mapping

(Figure 2a and 2b). Additionally, two-dimensional MoS_2 nanosheets also cannot be observed among the nanofibers (Figure 2c), but they can be detected and are well encapsulates in the matrix of CNFs (Figure 2d). After carbonization, the PAN molecules have transformed into amorphous carbon (Figure 2e), and the typical lattice fringes with an interplanar spacing of 0.63 nm are observed among the amorphous carbons (Figure 2f), indexed to the (002) facets of MoS_2 [20], which has the same characteristics as the exfoliated MoS_2 nanosheets (Figure S3). Figure 2g-j shows a typical scanning transmission electron microscopy (STEM) bright field image and elemental mapping analysis of the 1D MoS_2/CNFs, where carbon, molybdenum and sulfur species are all distributed in this area. More importantly, the free-standing 1D MoS_2/CNFs can be

Preprints (www.preprints.org) | NOT PEER-REVIEWED | Posted: 28 December 2016 doi:10.20944/preprints201612.0133.v1

easily cut into flexible tablet and directly used as binder-free anode for lithium-ion batteries (Figure S4).

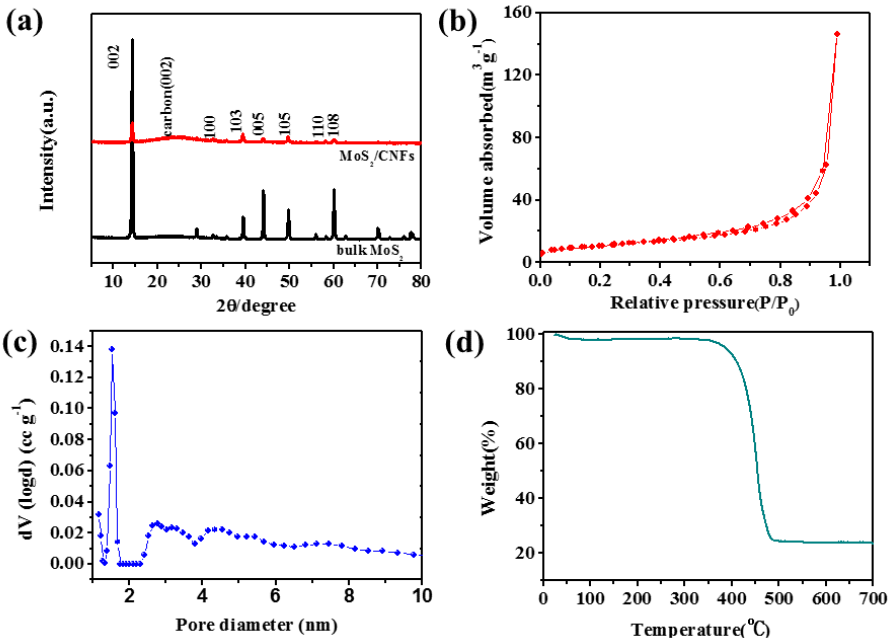

Figure 3. (a) XRD pattern of the resultant MoS_2/CNFs and bulk MoS_2 samples. (b) Nitrogen adsorption/desorption isotherms of the MoS_2/CNFs. (c) Pore diameter distribution of the MoS_2/CNFs. (d) TG curve of the MoS_2/CNFs

To further explore the chemical composition of the 1D MoS_2/CNFs, XRD measurement was performed. As shown in Figure 3a, there are several strong peaks at 14.2°, 32.6° and 39.6°, corresponding to the (002), (100), (103) planes of MoS_2[22]. It should be noted that the peak of MoS_2/CNFs at 14.2° is much weaker than that of bulk MoS_2, suggesting the bulk MoS_2 has been successfully exfoliated into two-dimensional nanosheets. There is a broad and weak peak at about 25°, which refers to the typical diffraction peak of amorphous carbon. There are no impurities are detected by XRD analysis, demonstrating the high crystallinity and phase purity of the resultant 1D MoS_2/CNFs. The type-IV hysteresis loop of the isotherm with pronounced adsorptions

Preprints (www.preprints.org) | NOT PEER-REVIEWED | Posted: 28 December 2016 doi:10.20944/preprints201612.0133.v1

was obtained at relative pressures P/P_0 from 0 to 1 (Figure 3b). The specific surface area of 1D MoS_2/CNFs was also obtained with 23.94 $m^2 g^{-1}$ on the basis of the nitrogen adsorption/desorption isotherms. Interestingly, the pore size distribution indicates that there exists micropores and mesopores in MoS_2/CNFs (Figure 3c), which should related to the layered and restacked MoS_2 nanosheets as well as the interlaced structure of CNFs. Thermogravimetric analysis was also performed to confirm the content of MoS_2 in the carbon nanofibers (Figure 3d). The weight loss occurs before 100 ºC, attributing to the evaporation of physically adsorbed water. The main weight loss occurs in the range of 300-500 ºC because of the consumption of carbon and the oxidation of MoS_2 to MoO_3 in air. According to the final yield of MoO_3, the content of MoS_2 encapsulated in the CNFs is more than 27.6%.

The elemental components and contents of 1D MoS_2/CNFs were elucidated by XPS measurement. Based on the XPS surveys, it is distinct that carbon, molybdenum, sulfide and oxygen species are assumed in the MoS_2/CNFs (Figure 4a), and the detail contents are illustrated in Table S1. The fitted C1s peaks are demonstrated in Figure 4b, the peaks located at 284.5, 285.5 and 287 eV are related to C-C, C-O and C=C bonds of amorphous carbon, respectively[23]. The high-resolution Mo 3d spectrum can be fitted to three types at the binding energies of 236.7, 233.4 and 230 eV, corresponding to the Mo^{6+}, Mo $3d^{3/2}$ and Mo $3d^{5/2}$ peaks (Figure 4c). The Mo $3d^{3/2}$ and Mo $3d^{5/2}$ peaks represent to the Mo^{4+} in MoS_2. The Mo^{6+} may attribute to the existence of MoO_3 which is caused by the unavoidable surface oxidation of MoS_2 in carbonization process. The high-resolution S 2p spectrum can be fitted to two types at 164 and 162.7 eV,

Preprints (www.preprints.org) | NOT PEER-REVIEWED | Posted: 28 December 2016 doi:10.20944/preprints201612.0133.v1

corresponding to the S $2p^{1/2}$ and S $2p^{3/2}$ peaks, represent to the S^{2-} in MoS_2[18]. The O 1s peaks observed in the spectrum are mainly caused by the oxygen in the testing environment.

Figure 4 (a) XPS spectrum of the 1D MoS_2/CNFs. High-resolution XPS spectra of C 1s (b), Mo 3d (c) and S 2p (d)

The electrochemical performance of MoS_2/CNFs was primary tested by galvanostatic charge-discharge measurement at a current density of 100 mA g^{-1}. As shown in Figure 5a, two obvious potential plateaus during the first discharge are visible in case of the MoS_2/CNFs electrode. The plateau at ~1.1 V is caused by the intercalation

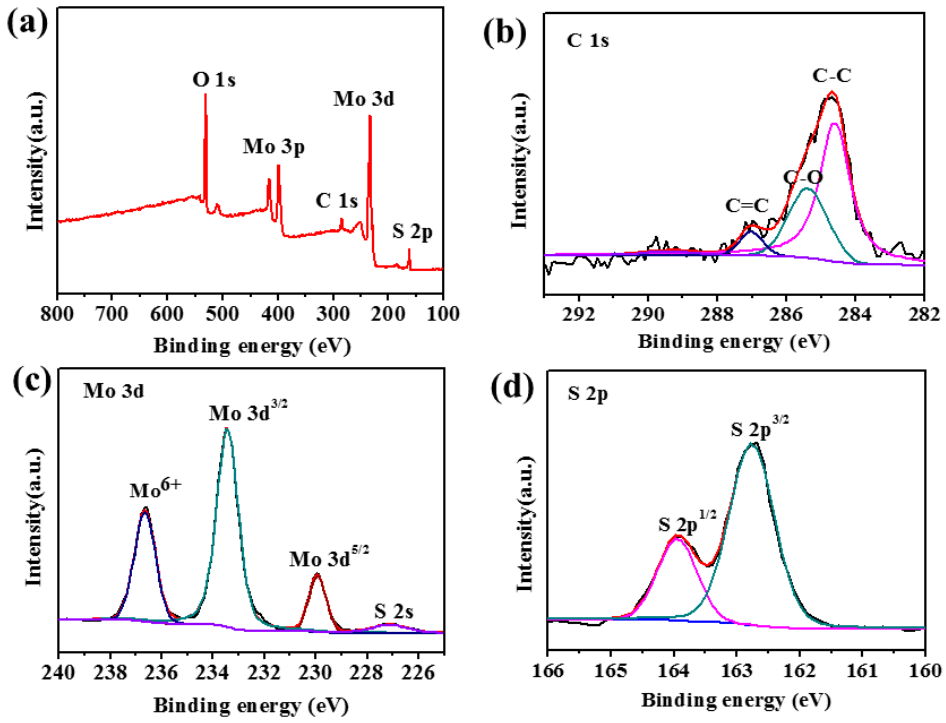

of Li^+ into MoS_2 to form Li_xMoS_2 which brings up the phase changing of MoS_2 from trigonal prismatic to octahedral. Another plateau at ~0.5 V is related to the conversion reaction of Li_xMoS_2 to Mo and Li_2S[24]. The initial discharge and charge capacity of MoS_2/CNFs electrode are1155 and 799 mAh g^{-1} at 100 mA g^{-1}, respectively, and the

 doi:10.20944/preprints201612.0133.v1

Coulombic efficiency is 69.2%. The irreversible capacity loss is mainly attribute to the formation of solid electrolyte interphase (SEI) film[25]. The reversible capacity of MoS_2/CNFs remains stable at 700 mAh g^{-1} at 100 mA g^{-1} after 50 cycles (Figure 5a), which is much higher than that of bulk MoS_2 (360 mAh g^{-1}, Figure 5b). Figure 5c indicates that the MoS_2/CNFs also shows better cycling performance than that of bulk MoS_2. For the exfoliated MoS_2 nanosheets, although the initial capacity is as high as1050 mAh g^{-1}, there is only 450 mAh g^{-1} after 50 cycles (Figure S4). The capacity fading is mainly caused by the restack and structure destruction of the MoS_2 nanosheets. A little capacity improvement could be observed in the result of MoS_2 nanosheets after some cycles, which should be contributed to the activation of Li^+ pathways between the electrolyte and electrode during cycling[26]. More importantly, the MoS_2/CNFs sample exhibits distinguished high-rate capabilities at different current densities from 50 to 1000 mA g^{-1} (Figure 5d). The reversible capabilities of MoS_2/CNFs sample is up to 530 and 450 mAh g^{-1} at 500 and 1000 mA g^{-1}, respectively, which are significantly higher than the contrast bulk MoS_2 (164 mAh g^{-1} at 1000 mA g^{-1}) and exfoliated MoS_2 nanosheets (148 mAh g^{-1} at 1000 mA g^{-1}, Figure S5). And when the current rate is again reduced back to 50 mA g^{-1}, the reversible capacity can be recovered and maintains at 769 mAh g^{-1}. In addition, the MoS_2/CNFs sample keep no attenuation at 1000 mA g^{-1}

Preprints (www.preprints.org) | NOT PEER-REVIEWED | Posted: 28 December 2016 doi:10.20944/preprints201612.0133.v1

after 200 cycles (Figure 5e), indicating the excellent long cycle performance.

Figure 5. Electrochemical performance of 1D MoS_2/CNFs for lithium-ion batteries. Charge-discharge curves of 1D MoS_2/CNFs (a) and bulk MoS_2 (b) at a current density

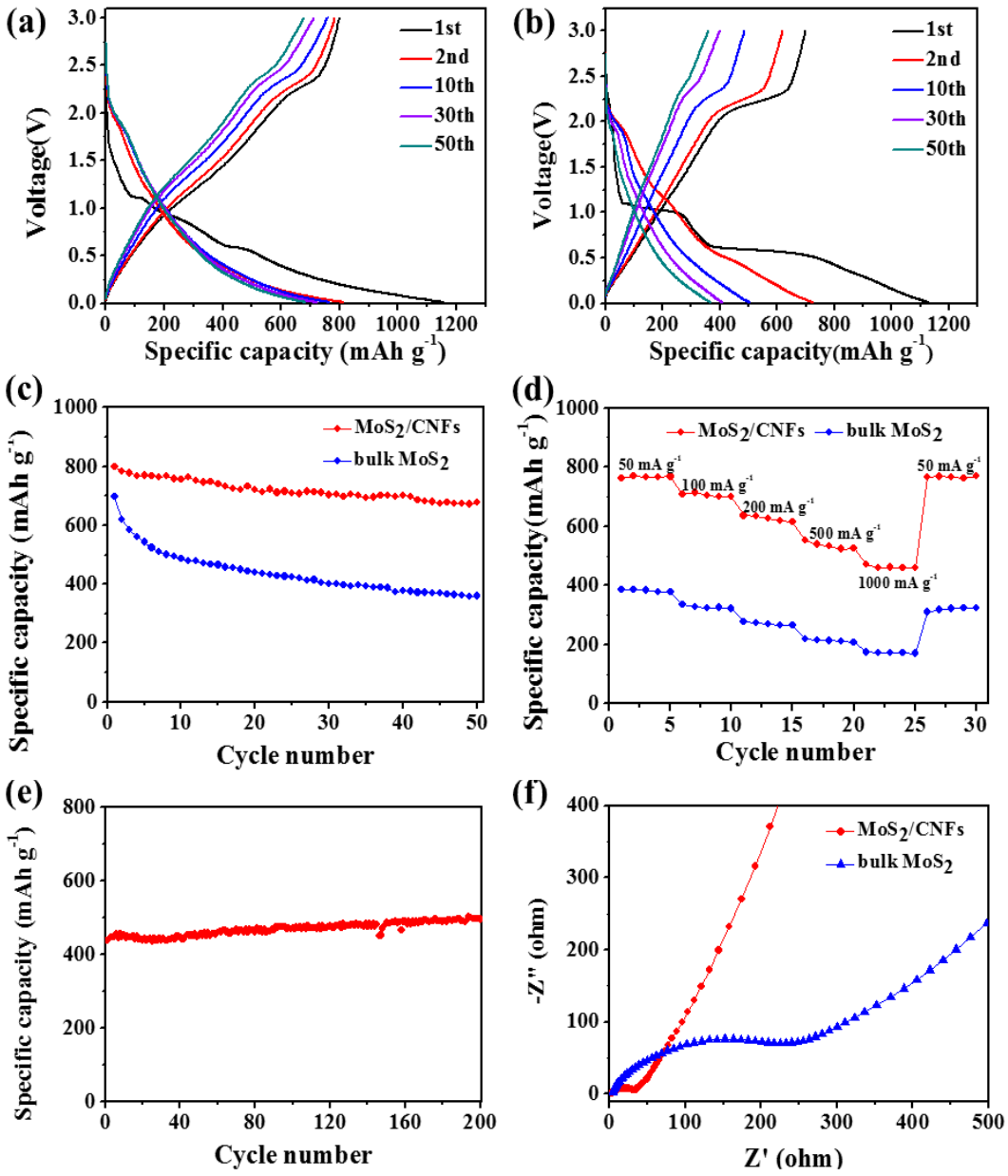

of 100 mA g^{-1}. (c) Cycling performance of bulk MoS_2 and MoS_2/CNFs at a current density of 100 mA g^{-1}. (d) High-rate performances of bulk MoS_2 and MoS_2/CNFs at various current densities of 50, 100, 200, 500 and 1000 mA g^{-1}. (e) Cycling performance of MoS_2/CNFs at a current density of 1000 mA g^{-1}. (f) Nyquist plots of bulk MoS_2 and

 doi:10.20944/preprints201612.0133.v1

MoS_2/CNFs after rate-cycling with an amplitude of 5 mV

To explore the reasons of the excellent electrochemical performance of the MoS_2/CNFs sample, the EIS measurement was employed after rate cycles and the equivalent circuit diagram of AC impedance was shown in Figure S6. The two plots both contains two semicircles which respectively locates at high and medium frequencies region and a straight line locates at low frequencies region. After data fitting, kinetic parameters collected in Table S2. The solid electrolyte interface resistance (R_f, 4.07 Ω) and charge transfer resistance (R_{ct}, 33.65 Ω) of MoS_2/CNFs are much lower than that of bulk MoS_2 (R_f,16.24 Ω; R_{ct}, 228.3 Ω). The fast diffusion of electron and high electrochemical activity for lithium storage in MoS_2/CNFs sample were clearly demonstrated by these results. The MoS_2 nanosheets homogenously encapsulated in the matrix of carbon nanofibers provide more active sites for lithium ions. The one-dimensional and small diameter microstructures of CNFs provide a short pathway for Li^+ transportation. And the intertwined CNFs form a well conductive network, which also play important role as a buffering effect to effectively decrease the volume expansion during charge-discharge cycling[27].

3. Experimental

3.1 Materials preparation

MoS_2 nanosheets were initially fabricated by a modified sheer exfoliation method as literature reported[21]. 90 mg exfoliated MoS_2 nanosheets were dispersed in 10 ml N,N-Dimethylformamide (DMF) by ultrasonication, then 60 mg polyacrylonitrile (PAN) were dissolved in the solution by stirring at 40 °C for 12 h. Subsequently, above

 doi:10.20944/preprints201612.0133.v1

mixture solution was poured into a syringe for electrospinning. Detailly, the diameter of the needle, the distance between needle and collector, the working voltage and the flow rate of the solution are 0.34 mm, 15 cm, 10 kV and 0.5 ml/h, respectively. Finally, the resultant 1D MoS_2/PAN nanofibers were oxidized at 280 ^oC in air for 2 h and then carbonized at 850 ^oC for 3 h under Ar atmosphere.

3.2 Materials characterizations

The morphologies of the samples are characterized by scanning electron microscopy (SEM, Zeiss MERLIN Compact) and transmission electron microscopy (TEM, JEOL 2100F). The structure and composition were characterized by X-ray diffraction (XRD, Rigaku D/MAX2500), X-ray photoelectron spectroscopy (XPS, Thermo Scientific Escalab 250Xi) and TGA (STA449 Jupiter, NETZSCH) measurements. The Brunauer-Emmett-Teller (BET) test was performed on a Quantachrome QDS-MP-30 analyzer (USA) at 77 K.

3.3 Electrochemical measurement

Electrochemical experiments were performed using standard CR2031 type coin cells assembled in the glovebox. After the MoS_2/CNFs was cut into flexible tablet, it was directly used as anode electrode. The exfoliated MoS_2 and bulk MoS_2 electrodes were fabricated by mixing the active material with acetylene black and poly(vinyl difluoride) (PVDF) at a weight ratio of 8:1:1. In the process of fabrication of lithium ion battery, pure lithium foil were used as counter electrode, propene polymer (PP) separator membrane as separate and 1 M $LiPF_6$ in ethylene carbonate as electrolyte. The galvanostatic discharge/charge behavior of coin cells was tested on a battery testing

 doi:10.20944/preprints201612.0133.v1

system (Land CT2001A) at the voltage of 0.01-3 V. Both cyclic voltammetry (CV) and electrochemical impedance spectrometry (EIS) tests were performed on Autolab equipment (PGSTAT302N).

4. Conclusions

We have developed an efficient approach to fabricate 1D MoS_2/CNFs by electrospinning. The free-standing MoS_2/CNFs can be easily cut into flexible tablet and directly used as binder-free anode for lithium storage. The unique structures offer the 1D MoS_2/CNFs a high gravimetric capacity (700 mAh g^{-1} at 100 mA g^{-1}) and good high-rate performance (450 mAh g^{-1} at 1000 mA g^{-1}) along with stable cycle property. We believe that this simple and efficient method can be further extended to fabricate various active anode material (such as transition metal oxides, Sn and Si, etc) encapsulated in one-dimensional carbon nanofibers or carbon nanotubes for broad applications in batteries, supercapacitors and catalysts.

Acknowledgment

This work was financially supported by National Science Foundation of China (Nos. 51472086, 51572007, 51622203, 51002051) and Recruitment Program of Global Experts (Nos. YWF-16-BJ-Y-12).

References

[1] Y. Huang, M. Zhu, Y. Huang, Z. Pei, H. Li, Z. Wang, Q. Xue, C. Zhi. Multifunctional energy storage and conversion devices. Adv. Mater. 2016, **28(38)**, 8344-8364.

[2] B. Luo, L. Zhi. Design and construction of three dimensional graphene based

composites for lithium ion battery applications. Energ. Environ. SCI. 2015,**8(2)**,456-477.

[3] X. Rui, H. Tan, Q. Yan. Nanostructured metal sulfides for energy storage. Nanoscale. 2014,**6(17)**,9889-9924.

[4] Y. Ma, H. Chang, M. Zhang, Y. Chen. Graphene-based materials for lithium-ion hybrid supercapacitors. Adv. Mater. 2015,**27(36)**, 5296-5308.

[5] M. Ebner, F. Geldmacher, F. Marone, M. Stampanoni, V. Wood. X-ray tomography of porous, transition metal oxide based lithium ion battery electrodes. Adv. Energy Mater. 2013,**3(7)**,845-850.

[6] L. Wan, W. Sun, J. Shen, X. Li. MgO-template-assisted synthesis of worm-like carbon@MoS_2 composite for lithium ion battery anodes. Electrochimica Acta. 2016, **211**, 962-971.

[7] D. H. Nam, T. H. Kim, K. S. Hong, H. S. Kwon. Template-free electrochemical synthesis of Sn nanofibers as high-performance anode materials for Na-ion batteries. ACS Nano. 2014, **8**, 11824-11835.

[8] L. Zhao, D.J. Dvorak, M.N. Obrovac. Layered amorphous silicon as negative electrodes in lithium-ion batteries. J. Power Sources. 2016, **332**, 290-298.

[9] Y. J. Zhai, J. H. Li, X. Y. Chu, M. Z. Xu, X. Li, X. Fang, Z. P. Wei, X. H. Wang. Preparation and application of molybdenum disulfide nanostructures. J. Inorg. Mater. 2015, **30(9)**, 897-905.

[10] H. Jiang, D. Ren, H. Wang, Y. Hu, S. Guo, H. Yuan, P. Hu, L. Zhang, C. Li. 2D monolayer MoS_2-carbon interoverlapped superstructure: engineering ideal atomic

 doi:10.20944/preprints201612.0133.v1

interface for lithium ion storage. Adv. Mater. 2015, **27(24)**, 3687-3695.

[11] C. Ahn, J. Lee, H. U. Kim, H. Bark, M. Jeon, G.H. Ryu, Z. Lee, G.Y. Yeom, K. Kim, J. Jung, Y. Kim, C. Lee, T. Kim. Low-temperature synthesis of large-scale molybdenum disulfide thin films directly on a plastic substrate using plasma-enhanced chemical vapor deposition. Adv. Mater. 2015, **27(35)**, 5223-5229.

[12] H. Y. Chang, M.N. Yogeesh, R. Ghosh, A. Rai, A. Sanne, S. Yang, N. Lu, S.K. Banerjee, D. Akinwande. Large-area monolayer MoS_2 for flexible low-power RF nanoelectronics in the GHz regime. Adv. Mater. 2016, **28(9)**, 1818-1823.

[13] G. Zhao, S. Han, A. Wang, Y. Wu, M. Zhao, Z. Wang, X. Hao. "Chemical weathering" exfoliation of atom-thick transition metal dichalcogenides and their ultrafast saturable absorption properties. Adv. Funct. Mater. 2015, **25(33)**, 5292-5299.

[14] H. Li, G. Lu, Y. Wang, Z. Yin, C. Cong, Q. He, L. Wang, F. Ding, T. Yu, H. Zhang. Mechanical exfoliation and characterization of single- and few-layer nanosheets of WSe_2, TaS_2 and $TaSe_2$. Small, 2013, **9(11)**, 1974-1981.

[15] X. Zhang, Z. Lai, C. Tan, H. Zhang. Solution-processed two-dimensional MoS_2 nanosheets: preparation, hybridization and applications. Angew. Chem. Int. Ed. 2016, **55(31)**, 8816-8838.

[16] Y. Liu, X. Wang, X. Song, Y. Dong, L. Yang, L. Wang, D. Jia, Z. Zhao, J. Qiu. Interlayer expanded MoS_2 enabled by edge effect of graphene nanoribbons for high performance lithium and sodium ion batteries. Carbon. 2016, **109**, 461-471.

[17] J. Ekspong, T. Sharifi, A. Shchukarev, A. Klechikov, T. Wagberg, E. Gracia-Espino. Stabilizing active edge sites in semicrystalline molybdenum sulfide by anchorage on

nitrogen-doped carbon nanotubes for hydrogen evolution reaction. Adv. Funct. Mater. 2016, **26(37)**, 6766-6776.

[18] H. Liu, X. Chen, L. Deng, X. Su, K. Guo, Z. Zhu. Preparation of ultrathin 2D MoS_2/graphene heterostructure assembled foam-like structure with enhanced electrochemical performance for lithium-ion batteries. Electrochimica Acta. 2016, **206**, 184-191.

[19] P.S. Toth, M. Velicky, M.A. Bissett, T.J.A. Slater, N. Savjani, A.K. Rabiu, A.M. Rakowski, J.R. Brent, S.J. Haigh, P. O'Brien, R.A.W. Dryfe. Asymmetric MoS_2/graphene/metal sandwiches: preparation, characterization and application. Adv. Mater. 2016, **28(37)**, 8256-8264.

[20] D. Xie, D.H. Wang, W.J. Tang, X.H. Xia, Y.J. Zhang, X.L. Wang, C.D. Gu, J.P. Tu. Binder-free network-enabled MoS_2-PPY-rGO ternary electrode for high capacity and excellent stability of lithium storage. J. Power Sources. 2016, **307**, 510-518.

[21] E. Varrla, C. Backes, K.R. Paton, A. Harvey, Z. Gholamvand, J. McCauley, J.N. Coleman. Large-scale production of size-controlled MoS_2 nanosheets by shear exfoliation. Chem. Mater. 2015, **27(3)**, 1129-1139.

[22] Y. Liu, X. He, D. Hanlon, A. Harvey, J.N. Coleman, Y. Li. Liquid phase exfoliated MoS_2 nanosheets percolated with carbon nanotubes for high volumetric/areal capacity sodium-ion batteries. ACS Nano. 2016, **10(9)**, 8821-8828.

[23] K. Zhou, W. Zhou, X. Liu, Y. Sang, S. Ji, W. Li, J. Lu, L. Li, W. Niu, H. Liu, S. Chen. Ultrathin MoO_3 nanocrystalsself-assembled on graphene nanosheets via oxygen bonding as supercapacitor electrodes of high capacitance and long cycle life. Nano

Energy. 2015, **12**, 510-520.

[24] J. He, P. Li, W. Lv, K. Wen, Y. Chen, W. Zhang, Y. Li, W. Qin, W. He. Three-dimensional hierarchically structured aerogels constructed with layered MoS2/graphene nanosheets as free-standing anodes for high-performance lithium ion batteries. Electrochimica Acta. 2016, **215**, 12-18.

[25] Y. Liu, N. Zhang, L. Jiao, J. Chen. Tin nanodots encapsulated in porous nitrogen-doped carbon nanofibers as a free-standing anode for advanced sodium-ion batteries. Adv. Mater. 2015, **27(42)**, 6702-6707.

[26] C. Zhao, J. Kong, X. Yao, X. Tang, Y. Dong, S.L. Phua, X. Lu. Thin MoS_2 nanoflakes encapsulated in carbon nanofibers as high-performance anodes for lithium-ion batteries. Acs Appl. Mater. Inter. 2014, **6(9)**, 6392-6398.

[27] C. Zhu, X. Mu, P.A. van Aken, Y. Yu, J. Maier. Single-layered ultrasmall nanoplates of MoS_2 embedded in carbon nanofibers with excellent electrochemical performance for lithium and sodium storage. Angew. Chem. Int. Ed. 2014, **53(8)**, 2152-2156.